2001-03

2-D modeling of GaN HEMTs incorporating the piezoelectric effect

Eimers, Karl P.

Monterey, California. Naval Postgraduate School

http://hdl.handle.net/10945/2751

NAVAL POSTGRADUATE SCHOOL
Monterey, California

THESIS

2-D MODELING OF GaN HEMTS INCORPORATING THE PIEZOELECTRIC EFFECT

by

Karl P. Eimers

March 2001

Thesis Advisor: Todd R. Weatherford
Second Reader: Harry Dietrich

2-D MODELING OF GaN HEMTS INCORPORATING THE PIEZOELECTRIC EFFECT

Karl P. Eimers-Lieutenant, United States Navy
B.S., United States Military Academy, 1992
Master of Science in Electrical Engineering-March 2001
Advisor: Todd R. Weatherford, Department of Electrical and Computer Engineering
Second Reader: Harry Dietrich, Naval Research Laboratory

Gallium Nitride (GaN) High Electron Mobility Transistors (HEMTs) are microwave power devices that promise to revolutionize the capability of Navy radar systems. The Office of Naval Research is currently funding basic research of developing microwave power amplifiers for use in future radar systems. This thesis incorporates piezoelectric (PZ) equations in the Silvaco Atlas^{TM} software for modeling GaN/AlGaN structures. The PZ effect enhances a two dimensional electron gas at the GaN/AlGaN interface due to stress induced polarization.

DoD KEY TECHNOLOGY AREAS: Electronics, Materials, Processes, and Structures, Modeling and Simulation

KEYWORDS: Gallium Nitride, High Electron Mobility Transistor, Piezoelectric Effect

13. ABSTRACT *(maximum 200 words)*

Gallium Nitride (GaN) High Electron Mobility Transistors (HEMTs) are microwave power devices that promise to revolutionize the capability of Navy radar systems. The Office of Naval Research is currently funding basic research of developing microwave power amplifiers for use in future radar systems. This thesis incorporates piezoelectric (PZ) equations in the Silvaco Atlas^{TM} software for modeling GaN/AlGaN structures. The PZ effect enhances a two dimensional electron gas at the GaN/AlGaN interface due to stress induced polarization.

14. SUBJECT TERMS Gallium Nitride, High Electron Mobility Transistor, Piezoelectric effect			**15. NUMBER OF PAGES**
			16. PRICE CODE
17. SECURITY CLASSIFICATION OF REPORT Unclassified	**18. SECURITY CLASSIFICATION OF THIS PAGE** Unclassified	**19. SECURITY CLASSIFICATION OF ABSTRACT** Unclassified	**20. LIMITATION OF ABSTRACT** UL

THIS PAGE INTENTIONALLY LEFT BLANK

2-D MODELING OF GaN HEMTS INCORPORATING THE PIEZOELECTRIC EFFECT

Karl P. Eimers
Lieutenant, United States Navy
B.S., United States Military Academy, 1992

Submitted in partial fulfillment of the
requirements for the degree of

MASTER OF SCIENCE IN ELECTRICAL ENGINEERING

from the

**NAVAL POSTGRADUATE SCHOOL
March 2001**

Author: _____
Karl P. Eimers

Approved by: _____
Todd Weatherford, Thesis Advisor

_____
Harry Dietrich, Second Reader

_____
Jeffrey B. Knorr, Chairman
Department of Electrical and Computer Engineering

iii

THIS PAGE INTENTIONALLY LEFT BLANK

ABSTRACT

Gallium Nitride (GaN) High Electron Mobility Transistors (HEMTs) are microwave power devices that promise to revolutionize the capability of Navy radar systems. The Office of Naval Research is currently funding basic research of developing microwave power amplifiers for use in future radar systems. This thesis incorporates piezoelectric (PZ) equations in the Silvaco ATLAS^{TM} software for modeling GaN/AlGaN structures. The PZ effect enhances a two dimensional electron gas at the GaN/AlGaN interface due to stress induced polarization.

THIS PAGE INTENTIONALLY LEFT BLANK

TABLE OF CONTENTS

THIS PAGE INTENTIONALLY LEFT BLANK

LIST OF FIGURES

THIS PAGE INTENTIONALLY LEFT BLANK

LIST OF TABLES

THIS PAGE INTENTIONALLY LEFT BLANK

ACKNOWLEDGMENTS

EXECUTIVE SUMMARY

A computer model of Gallium Nitride (GaN) High Electron Mobility Transistors (HEMTs) has been developed for the purpose of designing and modifying high power and high frequency power amplifiers. GaN HEMT power amplifiers are being investigated for the Advanced Multi-function RF System (AMRFS). This model includes the impact of the piezoelectric effect automatically based on the material parameters of the GaN HEMT.

The piezoelectric effect results from the GaN noncentrosymmetric crystal combined with strain induced at the AlGaN/GaN heterojunction by lattice mismatch. This effect results in a predictable amount of electron sheet charge at the heterojunction providing exceptional conductivity of electron current. GaN material offers large energy bandgap, high breakdown voltage, and high peak electron velocity. The heterojunction also produces a quantum well which further enhances the speed of electron transport from source to drain contacts.

Silvaco software was modified to incorporate these physical realities. Equations generated by Prof. Ambacher of Cornell University utilize the mole fraction of Aluminum in the AlGaN layer and the thickness of that layer to accurately predict the resultant amount of two dimensional electron gas (2-DEG). The software modifications use that result and simulate implanting an appropriate amount of donor impurities in the top 10 nanometers of GaN material that lies directly below the AlGaN layer. The software incorporates these calculations when first generating the device for simulation. Once the software begins executing voltage biasing commands, electron mobility and electron saturation velocity values are manually controlled to avoid the expected scattering effects that impurity implantation would normally instigate.

Simulations were run on a model based on actual devices produced and tested at the Naval Research Laboratory (NRL). Various levels of Aluminum mole fraction were tried and resulted in electron concentrations expected by the Ambacher equations. Electron concentrations were found to match the program generated donor implantation within 4% accuracy. Energy band diagrams were generated to verify proper electron energy levels expected for a HEMT device. The program proved capable of matching expected energy band profiles throughout various mole fraction levels.

A model based on NRL's devices with a matching mole fraction was run through drain-to-source bias conditions and compared with measured results provided by NRL. The device was simulated under matching gate biases and I-V curves presented to show a general correspondence between modeled and measured results. Numerous combinations of electron mobility and velocity saturation were tried to improve model accuracy. Results presented derive from a simulation run with reported values of mobility and velocity saturation. Possibilities for improving model accuracy are discussed and evaluated for further research.

This work is the only reported software model that incorporates the piezoelectric effect. GaN HEMT performance is strongly related to the piezoelectric effect which governs the amount of charge carriers available in the device. Since the GaN HEMT promises to be the most powerful available high frequency power amplifier, it is hoped this work will be an important step forward in realizing the potential of this new device.

THIS PAGE INTENTIONALLY LEFT BLANK

I.   INTRODUCTION

A.   BACKGROUND

Radio Frequency (RF) amplifiers are vital to Navy technology requirements. The Navy employs many systems that radiate RF energy for communication, navigation, or detection and ranging. RF waveforms used by these systems are typically formed by delicate mechanisms at minimal power; so, virtually every RF emission is amplified before transmission. Often this amplification has been done by travelling-wave tube (TWT) technology, which is expensive and readily degrades over time.

Solid state amplifiers offer a promising alternative to TWTs. Incorporating smaller size and higher reliability, semiconductor amplifiers offer easier manufacturing, packaging, and handling than tubes. These amplifiers cannot currently match the maximum amplification of TWTs, yet they demonstrate respectable power levels with less distortion than TWTs, especially over extended periods of time [1].

Field Effect Transistors (FETs) are excellent RF power amplifiers especially above 4 GHz and where low noise is particularly vital. Generally, FETs have superior power gains, lower noise, and higher output power capabilities than their chief competitor, the bipolar junction transistor (BJT) [2]. The FET benefits in speed and noise from its single carrier (unipolar) process.

High Electron Mobility Transistors (HEMTs) are the most promising high-speed power amplifiers yet seen. The HEMT, while a relatively immature technology, has the highest current-gain cutoff frequency yet measured for any semiconductor device. The HEMT uses an energy offset that occurs between the substrate material and its upper

layer of Aluminum alloy (which is doped in a special way; this modulated doping gives rise the HEMT's other name, the MODFET). Since the GaN substrate material is nearly or completely undoped, the highest possible electron mobility and least amount of scattering are achieved.

Non-Silicon semiconductors dominate the high power, high frequency amplifier environment. Compound semiconductors such as Gallium Arsenide are more difficult to manufacture but offer advantages in material parameters such as electron mobility allowing greater gain and faster operation. Gallium Nitride (GaN) is a different compound semiconductor that has promise to be the ultimate in RF amplification because of its high frequency and high temperature capability and extremely high power output.

Software modeling is a versatile tool for designing and analyzing semiconductor devices. Parameters that can be calculated include DC characteristics such as threshold voltage, gain, leakage, punch through voltage and breakdown behavior. RF characteristics that can be predicted include cut-off frequency, s-, y-, h- and z-parameters, maximum available gain, maximum stable gain, maximum frequency of oscillation and stability factor. Intrinsic switching times and Fourier analysis of periodic large-signal outputs can also be calculated.

High power GaN microwave devices require special attention for accurate modeling. Heat is a crucial parameter in predicting device performance for high-power, high-speed devices.   The piezoelectric (PZ) effect has never been modeled in a Technology Computer Aided Design (TCAD) program yet may be the key to designing GaN-based compound semiconductor devices.   The PZ effect refers to the physical property of some materials, GaN in particular, to exhibit polarization when strained. This

polarization results in lowered resistivity due to the presence of extra charge carriers. Since GaN and AlGaN have a slight lattice mismatch, every HEMT structure exhibits the PZ effect. Adding mechanical strain to a device might further enhance PZ effect.

B.   RELATED WORK

The Naval Research Laboratory is currently conducting research on GaN HEMT power amplifiers. They are using Silvaco Software to model devices that they have built or intend to build. NRL's models do not automatically account for the piezoelectric effect. This work hopes to dovetail their efforts and take a further step in accurately replicating the GaN HEMT.

UC Berkeley is conducting tests of compound semiconductor materials to include Gallium Nitride. They are conducting tests that apply mechanical stress to materials and measuring various constants related to the piezoelectric effect. Their testing of GaN and AlGaN materials under applied stress could assist in accurately modeling externally applied stress effects. This work currently focuses on internal stresses generated by lattice mismatch between AlGaN and GaN heterojunctions.

C.   OBJECTIVES

This work seeks to increase the Navy's capability to model GaN HEMTs by providing a working Silvaco Software model of an existing GaN HEMT device. The model developed is distinguished in that it incorporates the piezoelectric effect.

THIS PAGE INTENTIONALLY LEFT BLANK

II. TRANSISTOR OVERVIEW

The following sections describe the basic structure and operation of field effect transistors and the high electron mobility transistor.

A. FIELD EFFECT TRANSISTOR

The FET was the original transistor, or transfer resistor, despite the earlier maturing of the bipolar junction transistor. The FET was first conceived in the 1920's, but it was not seriously developed until the 1960's. In between those time periods, the BJT emerged and blossomed into an effective electronic component. Regardless of temporarily losing prominence to the BJT as the electronic device of choice, the FET has regained distinction by its compactness and by easier production. Thanks to the computer industry, the FET (specifically the MOSFET) is currently the most produced manmade object in the world [3].
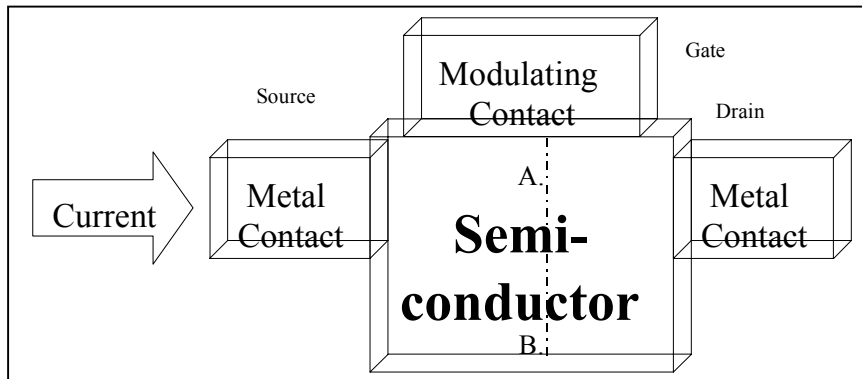
Figure 1. Basic FET structure.

The FET operates by separating metal contacts (source and drain) by a piece of semiconductor. Another contact (non-conducting gate) modulates the conductance/resistance of the semiconductor material by applying a voltage and thereby modulating the current flow between the original two contacts. As shown in Figure 1,

electric current entering the FET can either be allowed to flow through, be restricted, or be shut off depending on the voltage applied at the modulating contact.

This device works because the modulating contact voltage controls the amount of depletion region present in the semiconductor. In order to induce current flowing in the semiconductor, a voltage difference must exist between the source and drain. The gate to drain voltage difference will cause a depletion region (or an inversion layer) to build around the modulating gate contact (which is grounded). If the modulating contact is biased opposite the voltage difference between the other contacts, the depletion region grows. As soon as a depletion region completely covers, or pinches off the channel of current carriers, the amount of current flowing from source to drain is limited to its existing level. If no voltage difference exists between the contacts, and the modulating contact is biased enough to create a complete depletion region, then the device is shut off (applying bias to the drain will cause no drain current).

Band diagrams allow us to see what is happening in the energy related aspects in the semiconductor material. With no bias at the modulating contact (also known as the gate contact) and no bias at the other contacts (the source and drain contacts), the three dimensional conduction band energy diagram looks like Figure 2.

The left rectangle (purple and 0.0 volts) is the first ohmic contact (the source). Without any bias applied anywhere on the device, the source contact mirrors its opposite contact, the drain, in having the lowest energy levels available. This is expected since the source and drain are ohmic (low resistance) contacts that allow electrons to flow from the semiconductor to the metal. Since an electron will seek the lowest energy state available,

any electron dropped onto the energy diagram of Figure 2 will naturally move to the source or drain contact.
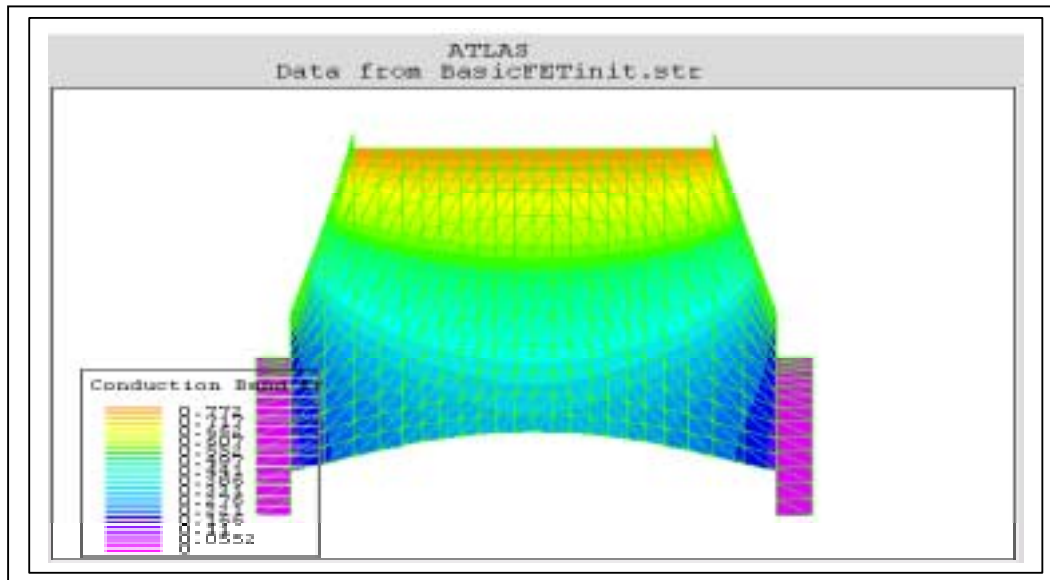
Figure 2. Energy band diagram for FET with no bias at gate contact.

The high-energy center of Figure 2 is the gate, which is a rectifying contact that prevents electrons from flowing into the gate. Changing the gate bias allows control of the energy band `blanket'. To cause current to flow through the device, bias is applied to the drain that pulls the blanket down on the right side of Figure 2. All electrons in the device naturally flow to the right finding the lowest energy state available. If one were to raise the gate voltage/energy level, the blanket would rise throughout the center of the device, especially close to the gate contact. The electrons would be forced to the bottom of the device restricting their flow. If enough gate bias were applied, all electrons from the source could be blocked from traveling through the semiconductor to the drain (regardless of how low the drain is biased).

B.   HIGH ELECTRON MOBILITY TRANSISTOR

First constructed by Mimura, et al., in 1980 [14], the HEMT is a different form of the field effect transistor but similar in structure to the MOSFET. It exploits the properties of non-Silicon semiconductors such as Gallium Arsenide and Gallium Nitride, specifically the electron transport properties of these compound semiconductors. The HEMT requires special deposition techniques such as molecular beam epitaxy (MBE) to grow a layer of Aluminum alloy (AlGaAs or AlGaN) on the undoped substrate. The Aluminum alloy layer is doped and acts as an insulator in the HEMT device (just like the oxide in the MOSFET).
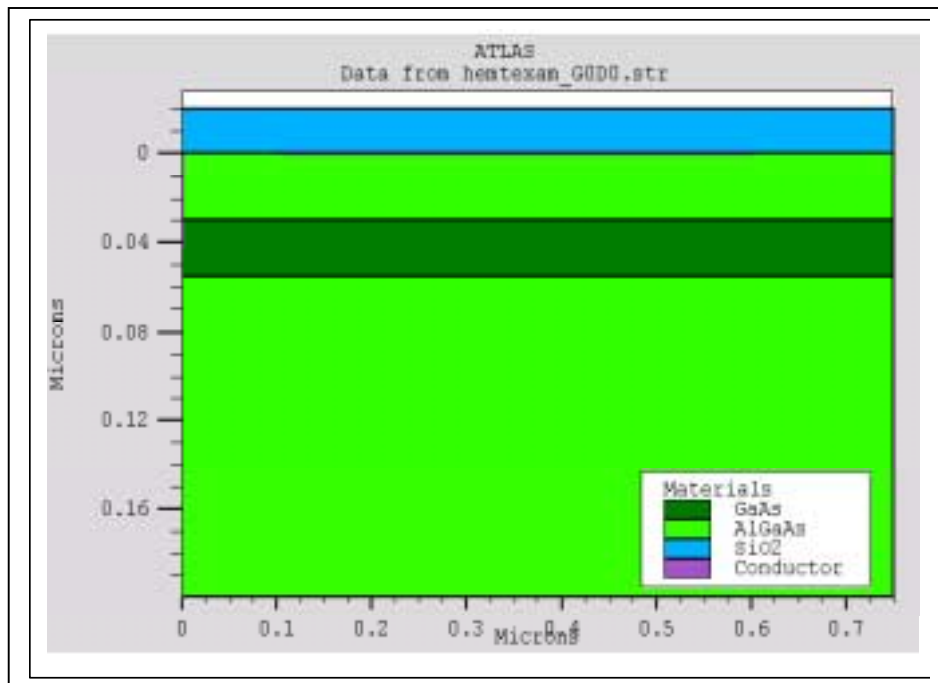
Figure 3. A HEMT or MODFET structure (From: Silvaco Software example files).

Depicted in Figure 3, the HEMT is also known as the modulation doped FET (MODFET) because the dopant source is modulated to selectively dope the Aluminum alloy layer. This helps induce a surface channel adjacent to the alloy-substrate interface. Since the channel is undoped, the electrons experience very little scattering in the surface

8

channel and, hence, have very high mobility. The name HEMT derives from this effect, and the HEMT enjoys electron mobility higher than even the MESFET device (which is doped and suffers from more scattering).

The key to HEMT performance is the conduction band offset (ΔE_C) present at the alloy-substrate interface. The alloy material has a wider bandgap than the substrate. At the interface, the substrate conduction band is pulled down to the Fermi level, making the interface highly conductive. Moving deeper into the substrate, the conduction band rises and pushes electrons toward the interface. On the alloy side of the interface, the conduction band is much higher than the interface level keeping electrons physically at the interface. The interface is naturally an inversion layer where electrons collect and sometimes described as a quantum well. This inversion layer is called a two-dimensional
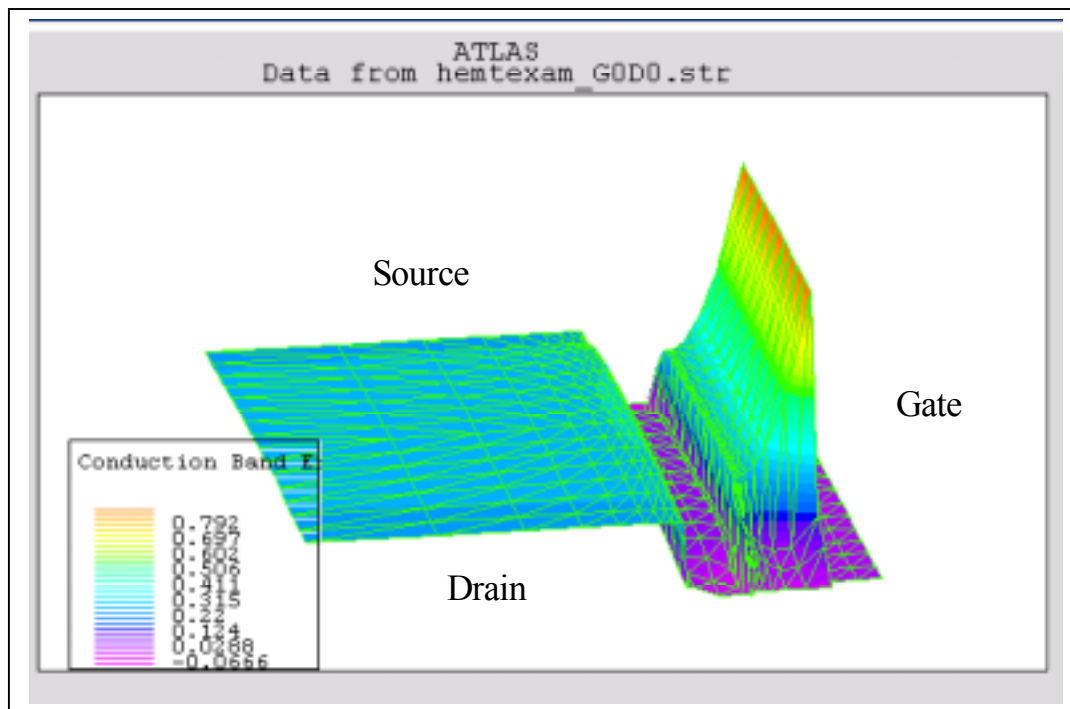
electron gas or 2-DEG.

Figure 4. Energy band diagram for unbiased HEMT device.

Figure 4 is a three-dimensional conduction band diagram of an unbiased HEMT viewed from the drain side. The ditch is the interface between the Aluminum alloy and the substrate where the ΔE_C and the 2-DEG appear. When a bias is applied to the drain, the energy band blanket is pulled down on the drain side requiring electrons to flow to its lower energy states, as in Figure 5. Application of gate bias can raise the energy levels through the center of the device and thereby modify the current flow as desired. A negative bias reduces the electron concentration in the channel and, if high enough, can completely repel electrons, turning the device off [15].
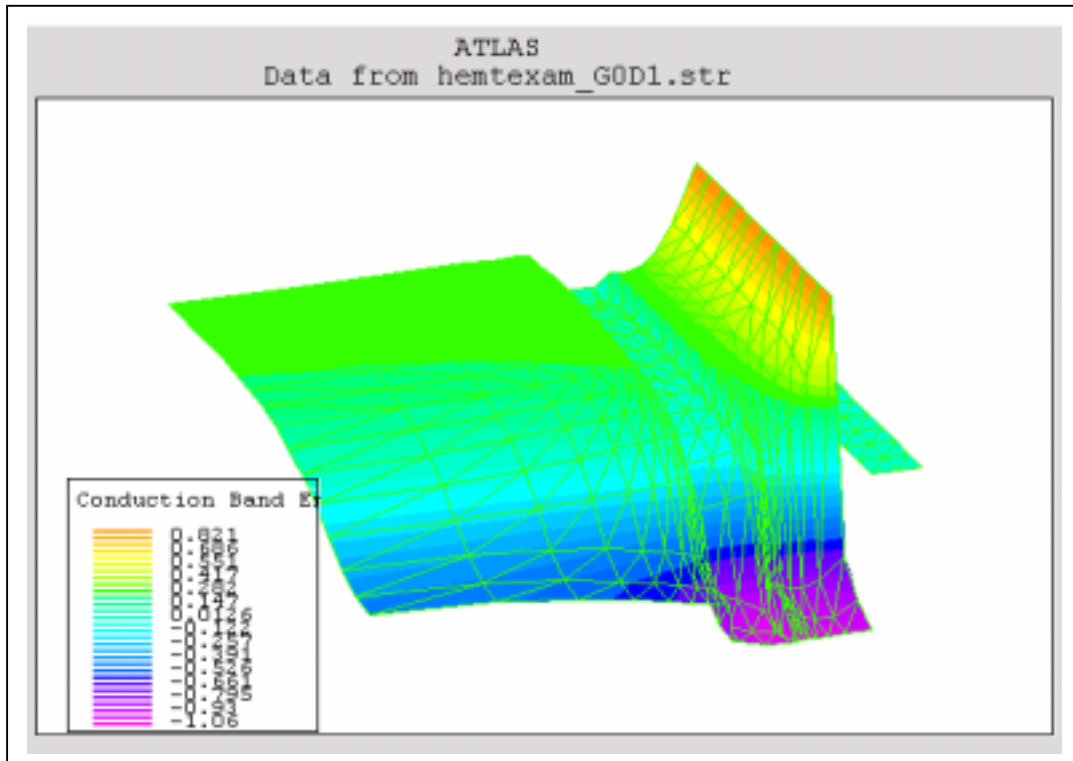
Figure 5. Energy band diagram for a HEMT with 2 volt bias at drain.

C.   GALLIUM NITRIDE

Group III-nitride materials are ideal for high power and high temperature devices due to their large energy bandgap, high breakdown voltage, high peak electron velocity

and high electron sheet density in channels when used in a heterostructure. Since most of the nitrides can form heterostructures and better ohmic contacts, they appear more promising than some contending materials such as Silicon Carbide. These wide bandgap materials are well suited to handle caustic and hostile environments such as high altitude or space. The nitrides also enjoy direct bandgaps making them very useful in optical applications.

The major drawback is difficulty of manufacture, especially in GaN devices, leading to problems in reliability and excessive cost. Much progress has been made in growth of quality Gallium Nitride crystals, but much is left to be done. Nitride materials have created difficulties in chemical etching due to its characteristically inert nature. They also have high melting temperatures and pressures making normal methods (such as Czochralski method) ineffective.

A problem for all high power devices is thermal dissipation. Higher temperatures degrade performance because low electric-field mobility and high electric-field electron velocity decrease with temperature. A successful substrate for GaN devices has been sapphire; however, Silicon Carbide can conduct heat at seven times the rate of sapphire [4]. Sapphire was the first successful substrate used with GaN by Shui Nakamura (who made a blue LED) at Nichia Chemical in Japan [5]. A better substrate material for GaN appears to be Silicon Carbide. SiC is a useful wide bandgap semiconductor in its own right, and much easier to fabricate. It boasts much better thermal conductivity than sapphire and a much closer lattice constant match (1% off GaN compared to 14% for sapphire and GaN). Sapphire continues to allure with its greatly reduced cost compared

11

to SiC. Other substrate candidates being investigated include Lithium Gallate and Neodymium Gallate.

D.   PIEZOELECTRIC EFFECT

The PZ effect is an electrical polarization produced by applying stress (internal or external) to the crystal. Many crystals exhibit the PZ effect to some degree and are used in devices that convert mechanical energy to electrical such as microphones, earphones, and accelerometers. Because AlGaN has a different lattice constant than GaN, in-plane biaxial stress is created when AlGaN is grown on GaN [6]. Studies have shown a direct relationship between the concentration of Al in the AlGaN layer to sheet charge density at the interface [7]. GaN and its compounds have very high piezoelectric constants resulting in values of piezoelectric fields that are measured in mega-Volts per centimeter. These high electric fields effect conductivity, allowing for electron transport without using dopants. Lattice mismatch is not the only way to introduce the required stress for PZ effect: mechanical force may be applied with similar effect.

GaN exhibits the PZ effect because it is a noncentrosymmetric crystal, that is, it has no center of symmetry in its unit cell. When atoms are pushed from their natural location, their charges do not balance equally. The demonstration of the PZ effect is shown in Figure 6. The left side displays an unstressed crystal, which exhibits some spontaneous polarization due to slightly unequal distribution of charged atoms. The right side displays the crystal stressed from top to bottom. This causes slight movement of the atoms increasing the unequalness of distribution and thereby increasing the total polarization. If the stress occurs in the direction of the spontaneous polarization, total

polarization increases.   Stress in the opposite direction would decrease the total

polarization [8].

Polarization [C/m^2] is used here in the sense of the volume density of an electric

dipole moment. This is typically observed in a dielectric material placed in an electric

field.   In a dielectric material the molecules experience a slight displacement so that

positive and negative charges line up in opposite directions which impacts the electric

field inside and outside the material. GaN and other noncentrosymmetric crystals exhibit

polarization with or without an externally applied electric field.
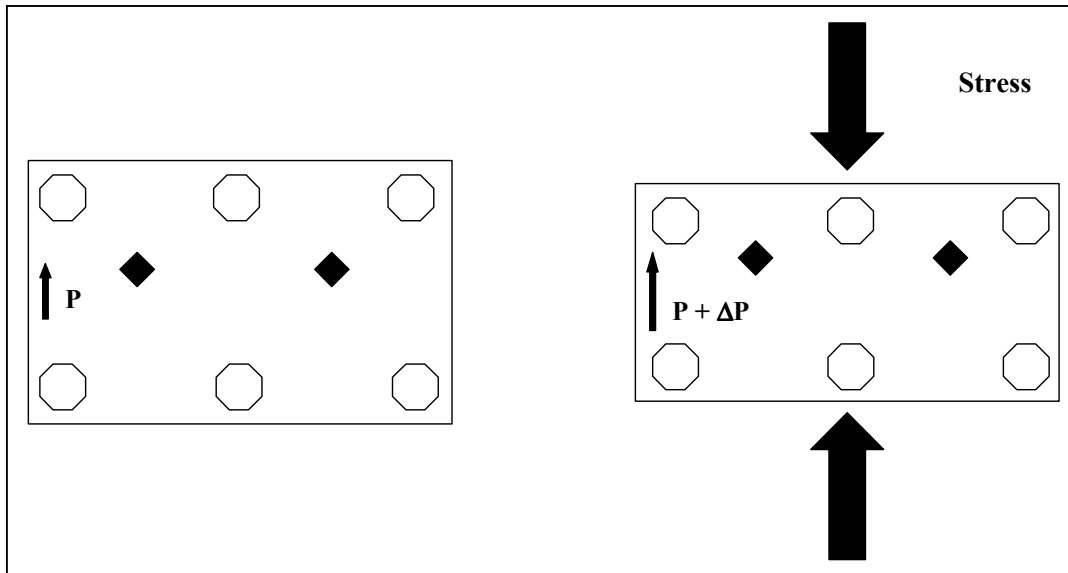
Figure 6. PZ effect demonstrated as increase in polarization due to mechanical stress.

The left side of Figure 6 shows a small polarization vector, **P**, which increases

with strain caused by the applied stress on the right side. The presence of **P** on the left

side is due to another quality of GaN: ferroelectricity. In a ferroelectric crystal, the center

of its positive charge (for GaN, the Nitrogen) does not coincide with the center of its

negative charge (the Gallium). This results in a net polarization even when unperturbed

by external forces (sometimes referred to as spontaneous polarization).   This

ferroelectricity, which is shared by many types of crystals, can result in a hysteresis loop

when electric field is applied and reversed slowly [9].

III. DEVICE MODELING

A. GENERAL

Silvaco International device simulation software performed the modeling in this work. Silvaco's ATLAS^{TM} program performed the general functions while BLAZE^{TM}, GIGA^{TM}, and C-INTERPRETER^{TM} performed specialized functions required for III-V/heterojunction devices, thermal calculations, and user defined equations, respectively. To control and modify the models, Silvaco's VWF Interactive Tools (specifically DECKBUILD^{TM}, TONYPLOT^{TM}, and DEVEDIT^{TM}) were utilized.

The Silvaco software uses physically based simulation rather than empirical modeling. While empirical modeling produces formulas that match existing data, physically based simulation predicts device performance based on physical structure and bias conditions. The Silvaco software represents a device on a two dimensional grid. At every grid intersection the program simulates carrier transport by means of differential equations derived from Maxwell's laws. To achieve accuracy, the program must incorporate the appropriate physics via numerical procedures. A brief description of those procedures follows in section B.

The device modeled for this thesis was created and tested by S. C. Binari (et al.) at the Naval Research Laboratory (NRL) in Washington, D.C. NRL continues to investigate GaN HEMTs expecting to exceed the performance of Gallium Arsenide transistors in high power applications.

B. NUMERICAL SIMULATION MODELS

To perform device simulation in the subject GaN HEMT, ATLAS uses Boltzmann statistics to describe carrier statistics. To correctly model III-V semiconductors, ATLAS employs the BLAZE program extension which modifies calculations that involve energy bands at heterojunctions. Heterojunctions require changes in calculating current densities, thermionic emissions, velocity saturation, and recombination-generation.

1. Boltzmann Approximation of Electron Probability

When modeling non-degenerate semiconductor material, the Fermi-Dirac statistical formula may be approximated as

$$f(\varepsilon) = \exp\left(\frac{E_F - \varepsilon}{kT_L}\right)$$

This provides the probability of an available electron state with energy E is occupied by an electron. E_F is the Fermi level; k is Boltzmann's constant; and T_L is the temperature. This formula is the basis for derivations that describe the effective density of states, the intrinsic carrier concentration, and the energy bandgap as discussed in [10]. These formulas will not be discussed.

2. Various

Several equations are not expounded here but appear in the Silvaco Software Manual [10]. Pertinent ones for this work include the energy balance equations, boundary (contact) physics, mobility model, carrier temperature dependent mobility, and carrier generation-recombination models.

3.   Solution Convergence

ATLAS uses these equations as it attempts to find solutions to carrier parameters such as current through the electrodes, carrier concentrations and electric fields throughout the device. ATLAS sets up the equations with an initial guess for parameter values then iterates through parameters to resolve discrepancies.   ATLAS will alternatively use a decoupled (Gummel) approach or a coupled (Newton) approach to achieve an acceptable correspondence of values.   When convergence on acceptable values does not occur, the program automatically reduces the iteration step size. ATLAS generates the initial guess for parameter values by solving a zero-bias condition based on doping profiles in the device.

C.   PIEZOELECTRIC EFFECT
1.   General

The primary research effort into the PZ effect has focussed on the internal strain caused by lattice mismatch between the AlGaN and GaN layers. The model developed in this work solely accounts for this internal strain.   Another factor that could be investigated is the amount of external stress or strain. We could enter either stress or strain, since stress is a measure of the force applied to something while strain is a measure of the deformation resulting from that stress. They are related by a single coefficient called the modulus of elasticity [11]. Applying an external (mechanical) stress to a device could increase or decrease the total PZ effect depending on the direction applied.

Also, an applied electric field might influence the total PZ effect. A piezoelectric crystal is essentially an electromechanical transducer that changes strain into electric potential and vice versa.   So, applying an external electric field will cause some

mechanical deformation which may further affect the total PZ effect. The question is, "Does this result in a measurable amount of sheet charge?"

Another parameter potentially important to high power devices is thermal expansion strain. This parameter is not ready to be modeled for several reasons. Current research has not uncovered reliable relationships because layer microstructure has no clear relationship to thermal strain. There is not enough evidence to demonstrate sample to sample consistency between GaN and sapphire or SiC. Finally, the Poisson coefficient is not reliably accurate and might be temperature dependent [12]. Given these uncertainties, thermal expansion will have to wait for more research before being incorporated into computer simulations.

2. Sheet Carrier Concentration due to Internal Stress

Sheet electron concentration may be calculated by:

$$n_S(x) = \frac{\sigma(x)}{e} - \left(\frac{\varepsilon_0 \varepsilon(x)}{d_{AlGaN} e^2} \right) \left[e\phi_b(x) + E_F(x) - \Delta E_C(x) \right] \qquad (1a)$$

Or

$$n_S(x) = \left\{ 1 + \frac{\varepsilon(x)}{\varepsilon(0)} \frac{d_{GaN}}{d_{AlGaN}} \right\}^{-1} \left\{ \frac{\sigma(x)}{e} - \left(\frac{\varepsilon_0 \varepsilon(x)}{d_{AlGaN} e^2} \right) * \left[e\phi_b^{eff}(x) + E_F(x) - \Delta E_C \right] \right\} \qquad (1b)$$

Ambacher [13] found that the dominant factor to describe sheet carrier concentration is the total polarization induced sheet charge which can be controlled by the alloy composition (the Al mole fraction) of the barrier. The sheet carrier concentration is directly related to the thickness of the Schottky barrier and inversely proportional to the height of the barrier.

The following physical properties can be calculated with x being the mole fraction of Al in the AlGaN layer ($Al_xGa_{(1-x)}N$):

Dielectric Constant

$$\varepsilon(x) = -0.3x + 10.4 \qquad (2)$$

The dielectric constant is normally assumed linear. This equation may be improved if future research provides a more accurate non-linear relationship.

Ni Schottky barrier

$$e\phi_b = (1.3x + 0.84)eV \qquad (3)$$

There are several types of metals used to make Schottky barrier contacts with GaN. Ni is a good choice for this work as its barrier height is comparable to most other candidates (as reported by Mohney in [17]) especially the Pt/Au used in the NRL HEMTs.

Band Offset

$$\Delta E_C = 0.7 \left[E_g(x) - E_g(0) \right] \qquad (4)$$

Band Gap

$$E_g(x) = (x6.13 + (1-x)3.42 - x(1-x)1.0)eV \qquad (5)$$

These equations hold true for values of x from 0.1 to 0.6.

The total bound sheet charge, $\sigma(x)$, is determined by the net polarization (PZ plus spontaneous).

The PZ polarization is:

$$P_{PE} = 2\{r(x) - 1\}\left[\frac{a_0(x) - a(GaN)}{a_0(x)}\right]\left(e_{31}(x) - e_{33}(x)\frac{C_{13}(x)}{C_{33}(x)}\right) \qquad (6)$$

Where r(x) is degree of relaxation, e is the PZ coefficient, a is the lattice constant and C is an elastic constant. These constants are also dependent on the mole fraction of Al:

$$a_0(x) = (-0.077x + 3.189)10^{-10}\, m \qquad (7)$$

a has the value of unstrained GaN, 3.189 Angstroms.

$$C_{13}(x) = (5x + 103)GPa \qquad (8)$$

$$C_{33}(x) = (-32x + 405)GPa \qquad (9)$$

$$e_{ij}(x) = \left(e_{ij}(AlN) - e_{ij}(GaN)\right) * x + e_{ij}(GaN) \qquad (10)$$

PZ coefficients for AlN and GaN were taken from [13] and determined to be AlN: e_{31} = -0.6 , e_{33} = 1.46 , and for GaN: e_{31} = -0.49 , e_{33} = 0.73.

The spontaneous polarization is:

$$P_{SP}(x) = (-0.052x - 0.029)\frac{C}{m^2} \qquad (11)$$

The relaxation degree for an AlGaN layer of 300 +/- 50 Angstroms, can be calculated by:

$$r(x) = \begin{cases} 0 & 0 \le x < 0.38 \\ 3.5x - 1.33 & 0.38 \le x \le 0.67 \\ 1 & 0.67 < x \le 1 \end{cases} \qquad (12)$$

Given these formulas for PZ and spontaneous polarization, the induced charge density can be calculated:

$$\rho_P = -\nabla P \qquad\qquad (13)$$

The value of the total bound sheet charge, $\sigma(x)$, required for equation (1), is calculated by:

$$\sigma(x) = \{P_{PE}(bottom) + P_{SP}(bottom)\} - \{P_{PE}(top) + P_{SP}(top)\} \qquad (14)$$

Where the bottom and top refer to the GaN and AlGaN layers in a horizontal heterostructure interface.

Ambacher states that the Fermi level is relative to the conduction band level in the GaN layer. He also states that it is dependent on the Al mole fraction of the AlGaN layer, however, he does not provide an equation to determine it. He does provide data that shows the sheet carrier concentration versus Al mole fraction. Using that information, one can calculate the Fermi level he used. Table 1 provides Ambacher's presented data, the Fermi level calculated from matching the equations to his data, the 2-DEG calculated from the previous Fermi level, the difference in the 2-DEG densities, and the Fermi level derived from the curve fit equation (which is used in this work's model).

Mole Fraction x	Ambacher 2-DEG X 10^{13}	$E_F(x)$ calculated eV	Calculated 2-DEG X 10^{13}	2-DEG error	$E_F(x)$ Modeled eV
0.1	0.263	0.1175	0.263	0.00%	0.116193
0.2	0.766	0.327	0.766	0.00%	0.334918
0.3	1.289	0.56	1.289	0.00%	0.54943
0.4	1.771	0.775	1.774	-0.17%	0.745028
0.5	1.921	0.86	1.921	0.00%	0.883491
0.6	1.892	0.875	1.889	0.16%	0.885441

Table 1. 2-DEG versus Fermi level.

Figure 7 demonstrates the correspondence of the calculated $E_F(x)$ with the modeled $E_F(x)$.
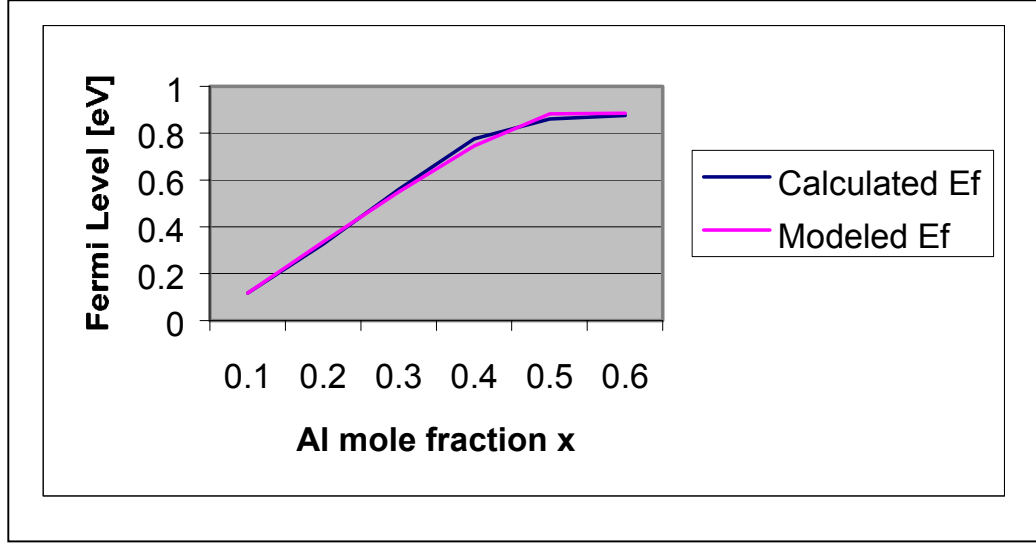
Figure 7. $E_F(x)$ calculated from Ambacher and $E_F(x)$ modeled for this work versus Al mole fraction.

The formula used to create the modeled $E_F(x)$ is:

$$E_F(x) = -0.102967 + (2.1917)x - (7)x^6 \qquad (15)$$

Table 2 contains all the variables (in three forms: Ambacher's; the ATLAS or BLAZE parameter; the C INTERPRETER argument), their source, and their function in the Silvaco code. All variables whose source is an equation are computed in Silvaco's C INTERPRETER.

VARIABLE (Ambacher/Silvaco equivalent parameter/C INT. argument)	SOURCE	PASSED IN/OUT
Sheet electron concentration n_S/NA/*fixed	Eq. (1)	Passed out
Al mole fraction X/x.composition/xcomp & ycomp	User & Structure file	Passed in
Dielectric constant ε/NA/*eps	Eq. (2)	Neither
Work function ϕ_b/WORKFUN/NA	Eq. (3)	Neither
Conduction band offset ΔE_C/ALIGN/NA	Eq. (4)	Neither
Bandgap E_g/EG300, EGALPHA, EGBETA/NA	Eq. (5)	Neither
PZ effect polarization P_{PE}/NA/NA	Eq. (6)	Neither
Lattice constant a_0/NA/NA	Eq. (7)	Neither
Elastic constant C_{13}/NA/NA	Eq. (8)	Neither
Elastic constant C_{33}/NA/NA	Eq. (9)	Neither
Piezoelectric coefficients ε_{13} & ε_{33}/NA/NA	Eq. (10)	Neither
Spontaneous Polarization P_{SP}/NA/NA	Eq. (11)	Neither
Degree of relaxation $r(x)$/NA/NA	Eq. (12)	Neither
Fermi level $E_F(x)$/NA/NA	Eq. (15)	Neither
Sheet charge $\sigma(x)$/NA/NA	Eq. (14)	Neither

Table 2. Variables, sources, and parameters.

Due to the nature of the Silvaco Software, the user must declare the values of the Al mole fraction and the thickness of the AlGaN layer in two locations. First, in the DEVEDIT structure file the AlGaN layer thickness is specified graphically which provides d_{AlGaN} (along with physical dimensions of every layer). The mole fraction in the AlGaN layer must also be specified (but as an impurity). The second specification of

these parameters occurs in the C-INTERPRETER code. This is required because one cannot make the C-INTERPRETER function input the depth of a layer nor the mole fraction (what C-INTERPRETER calls "xcomp") from a remote area. Since the doping function only checks conditions at the very point where it is placing the dopants (which is in the GaN layer), it must be told about the xcomp in the AlGaN layer. The C-INTERPRETER file is called by the DECKBUILD file listed in appendix A.

III.   RESULTS

A.   THE MODEL

A Silvaco model was generated based on the devices that have been built and tested by the Naval Research Laboratory. Figure 8 demonstrates the typical NRL HEMT as reported by Binari in [16].
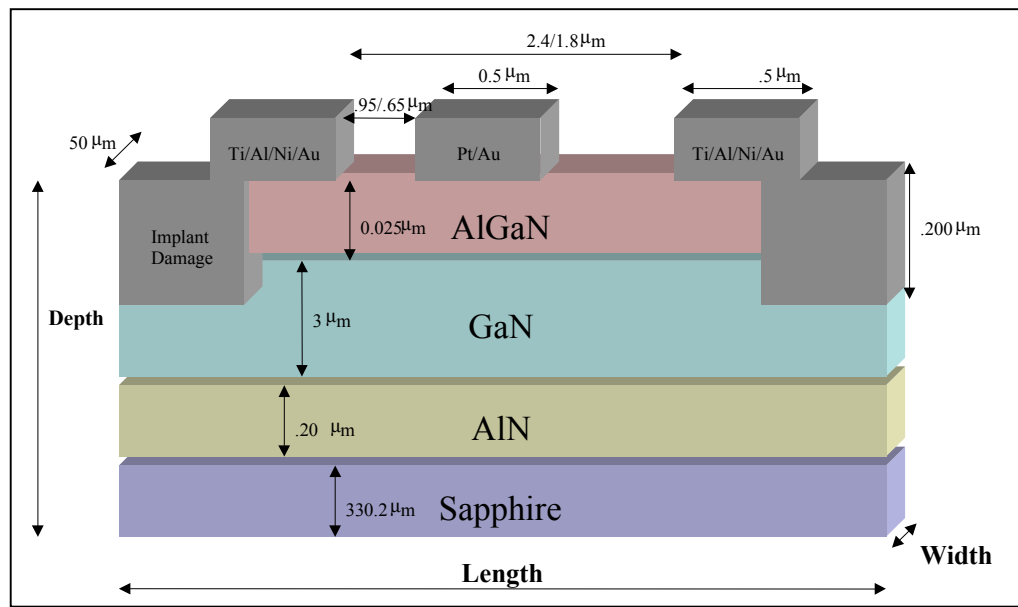
Figure 8. A typical NRL AlGaN/GaN HEMT.

The actual model is somewhat different as can be seen in Figure 9. The implant damage zones, which provide isolation in the real device, were not included and the source and drain contacts were placed directly on the GaN layer. This change in the contact placement is required to allow proper current flow from contacts to the device. If contacts are placed on the AlGaN layer, the software treats the layer as an effective insulator preventing any current flow.
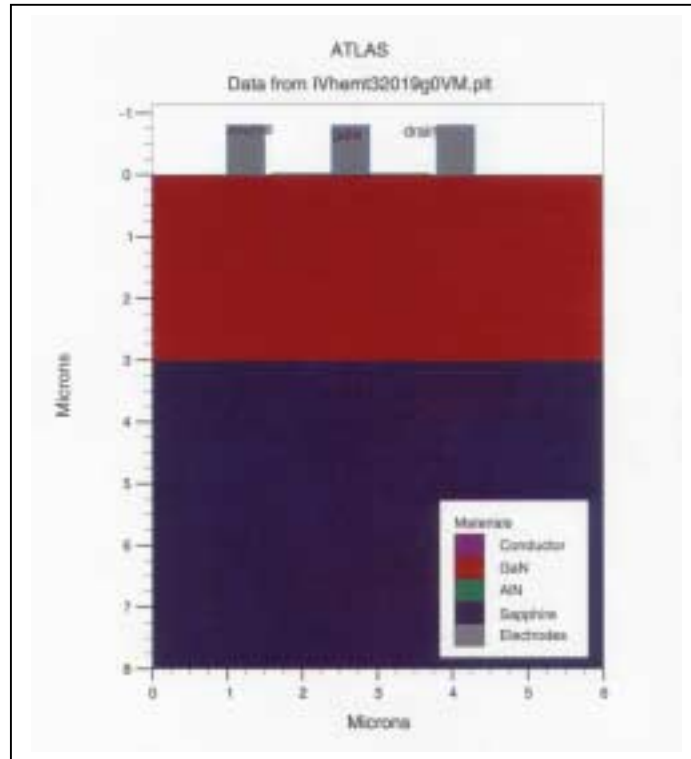
Figure 9. HEMT model created in Silvaco software.

Figure 10 provides a closer view of the contacts and heterojunction.
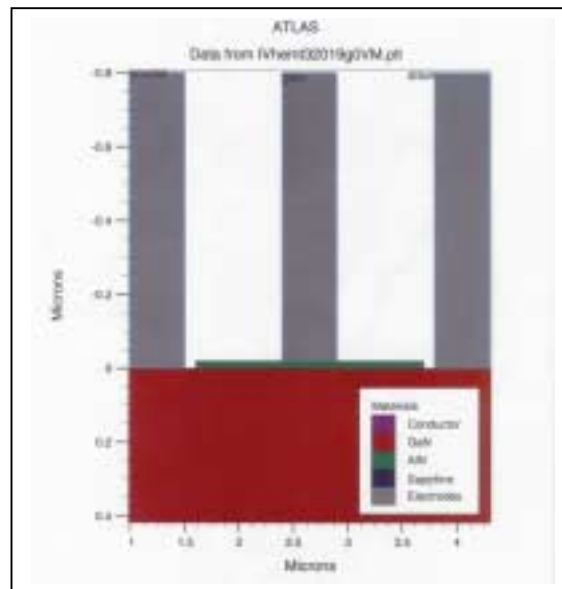
Figure 10. Close view of HEMT contacts from same model.

The layer beneath the gate contact is listed as AlN. This is because Silvaco does not allow AlGaN as a material. However, using the DEVEDIT program, this AlN layer can be assigned a mole fraction value (called "x comp") which is used by C-INTERPRETER to modify important parameters such as bandgap, electron affinity, conduction and valence bands density of states. In order to test the program, three simulations were run in different Aluminum mole fractions in the AlGaN layer. Values of 0.1, 0.3, and 0.5 were used to observe model behavior. Figure 11 demonstrates the varying bandgaps amongst these three trials.

B.   2-DEG
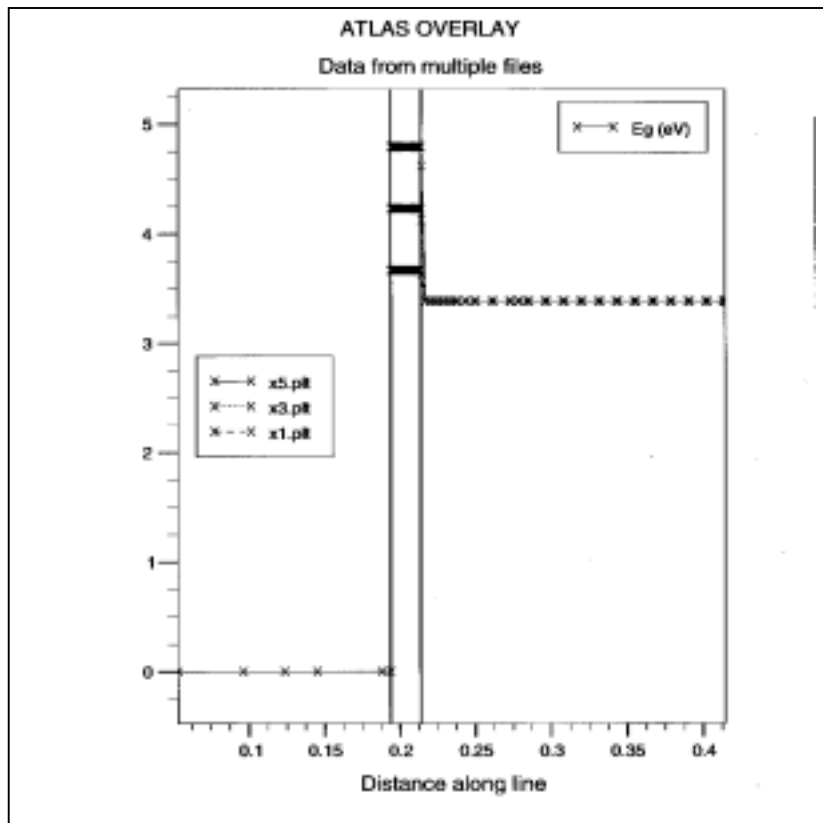
Figure 11. Bandgaps of various models.

Figure 11 is a cutline from the gate contact to the GaN layer. The left column is the gate contact which has a 0eV bandgap, the center column is the AlGaN layer, and the

right column is the GaN layer which has a 3.36eV bandgap (the expected value for intrinsic GaN). In the center column, the lowest line represents the X = 0.1 mole fraction in $Al_XGa_{(1-X)}N$. The middle line is X = 0.3; and the top is X = 0.5. Each line demonstrates the proper amount of bandgap for each alloy as they approach the large bandgap of AlN of 6.2 eV.

In order to create the 2-DEG, a C-INTERPRETER function called "f.doping" is used to place the appropriate number of electrons at the AlGaN/GaN interface. The appropriate level of electron concentration is determined by Ambacher's equations as represented by the C computer code in appendix B. The Ambacher equations generate a sheet charge in carriers per square centimeter. Since Silvaco accepts donor concentrations in dopants per cubic centimeter, the sheet charge is multiplied by one million to be spread over $1/100^{th}$ of a micron (that is: $[N_D/cm^2]$ x $(1/10^{-6}$ $[1/cm]))$.

The AlGaN layer is also doped in a manner appropriate to a MODFET. It is doped with 5e+18 from the top of the layer until 0.02 microns from the bottom. The last 0.02 microns are left undoped which gives the characteristic HEMT band structure to the AlGaN layer. The resultant doping for the three trials appears in Figure 12.
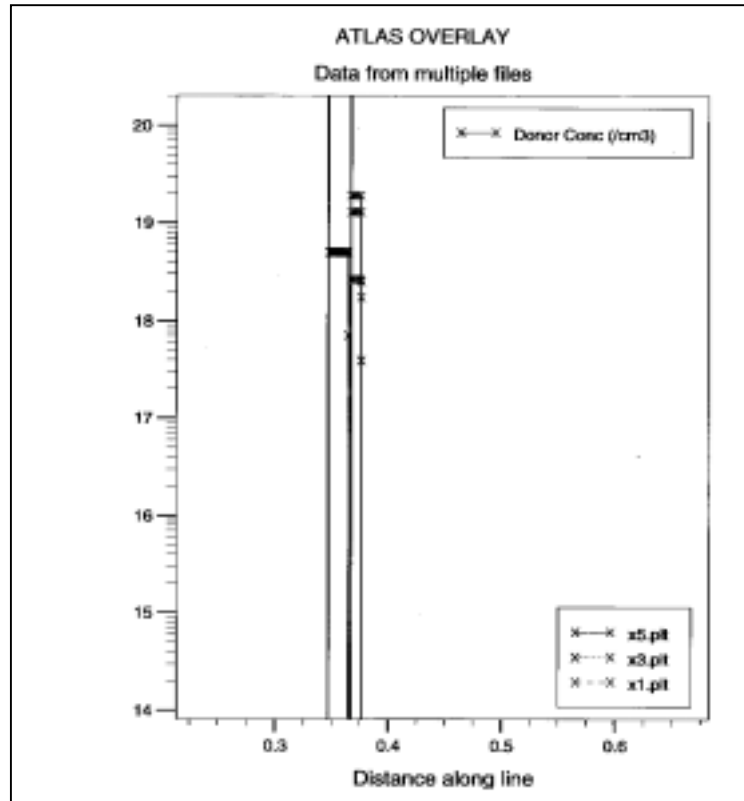
Figure 12. Donor concentration profile of various models.

As before, the left column is the gate which has no doping, the center is the AlGaN layer which is doped from the top (which in this perspective is the left side) to 0.2 microns from the bottom, and the GaN layer which has a spike of doping right at the AlGaN/GaN interface. Figure 13 zooms in to the interface spike.
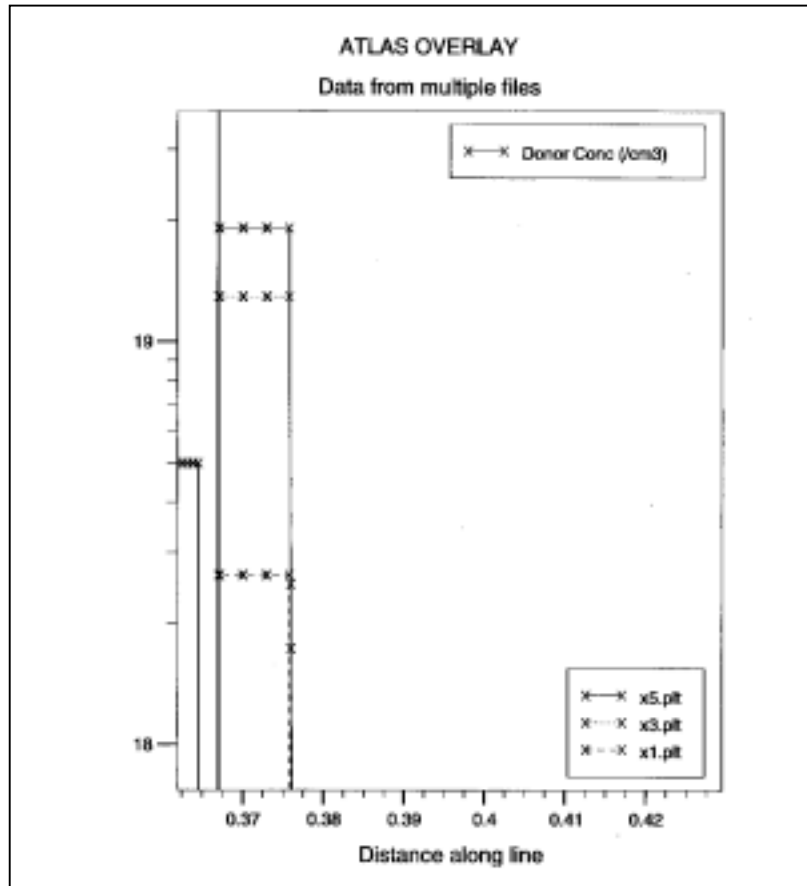
Figure 13. Donor concentration spike at interface of various models.

In Figure 13, three spikes can be seen. Each corresponds with the Al mole fraction of the model run. The 0.5 model demonstrates an approximate 2e+19 concentration, the 0.3 has approximately 1e+19, and the 0.1 has 2e+18. Since these numbers are in dopants per cm^3, they must be divided by one million to achieve the equivalent sheet density. These numbers become 2e+13, 1e+13, and 7e+12 and compare to Ambacher's predictions of 1.9e+13, 1.2e+13, and 2.6e+12.

These doping levels result in the desired concentrations of charge carriers as demonstrated in Figure 14.
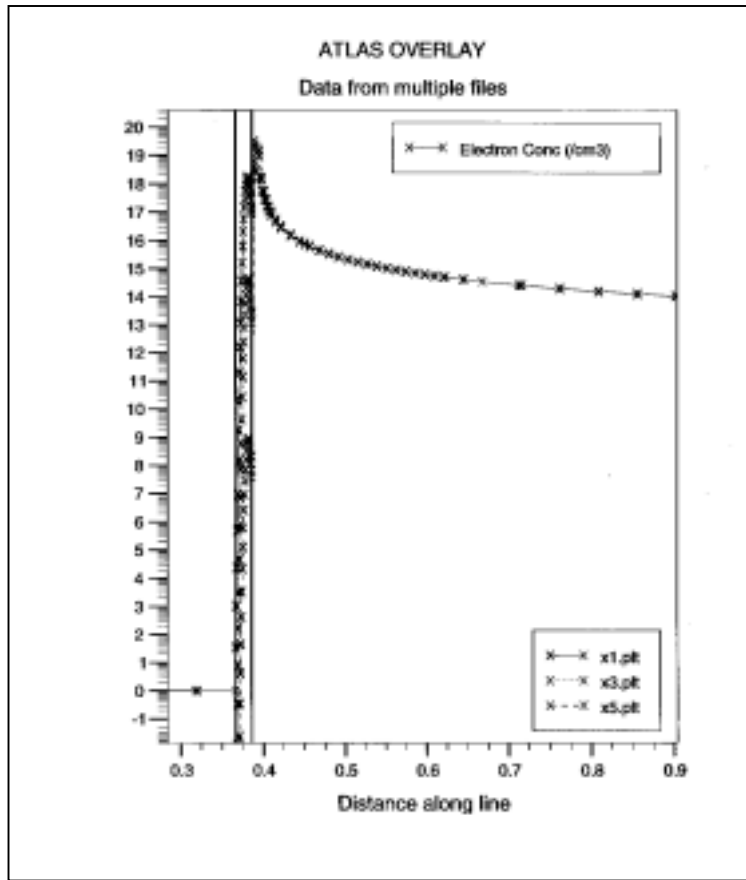
Figure 14. Electron concentrations versus distance of various models.

Figure 15 provides a close up of the spike of electrons at the AlGaN/GaN interface. This jump in electron concentration is the desired 2-DEG resulting from polarization.
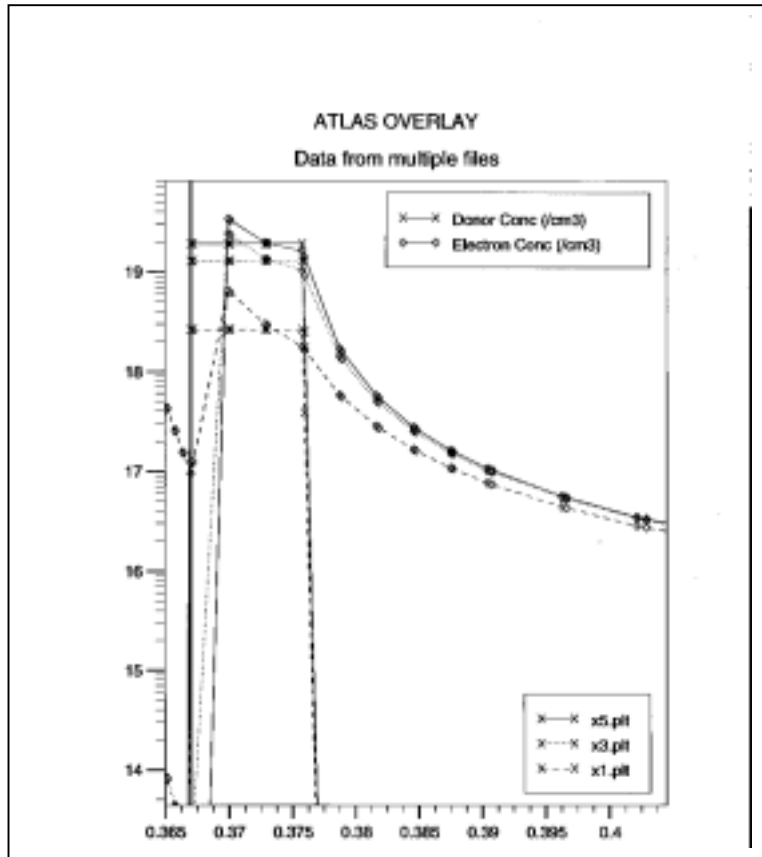
Figure 15. Electron concentrations at the interface of various models.

As can be seen in Figure 15, the amount of charge in the channel is approximately the same as the doping and what Ambacher predicts. This is the desired result of this thesis. Figure 15 provides both the electron concentration and the doping profile so that one can see that while the electron concentration exceeds the desired doping concentration, it does so only in a very reduced area. Using Silvaco's Integrate function in TONYPLOT, these two areas were found to differ by less than 4%.

The following figures show the energy bands of the device, again looking at a cutline from the gate through the AlGaN layer and into the GaN layer. They demonstrate the expected shape for a HEMT device as seen back in Figure 4.
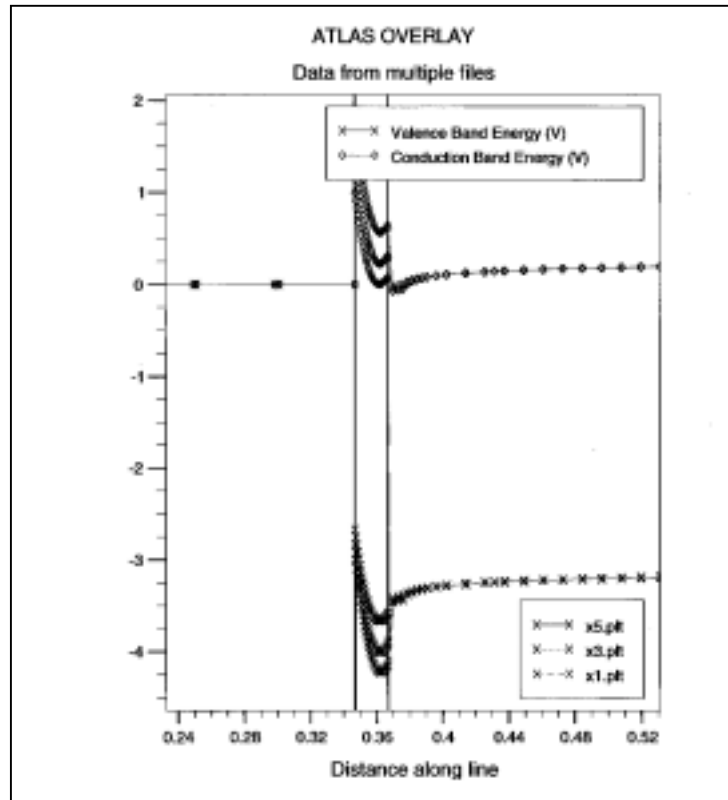
Figure 16. Conduction and valence band energy versus distance of various models.

Figure 16 shows the entire energy band diagram around the AlGaN layer while Figure 17 shows the conduction band more closely. Once can see the expected trench or quantum well that make the HEMT a unique transistor device. (Figures 12 through 17 all show the results from three models of different Aluminum mole fractions, as specified in the lower right corner. The demonstrated Aluminum mole fractions are x = 0.1, 0.3, and 0.5.)
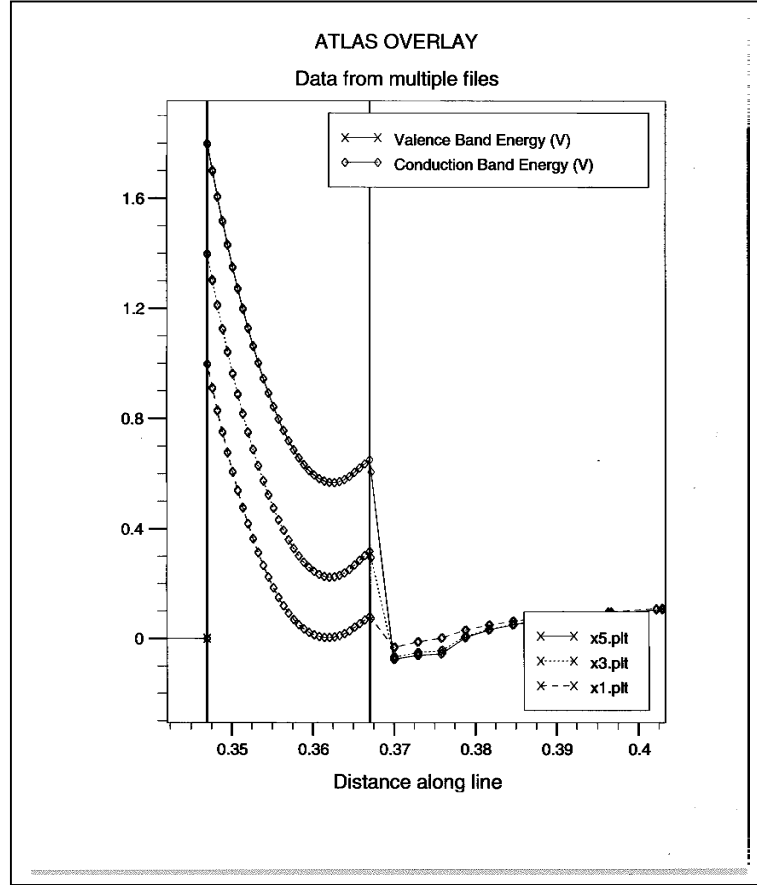
Figure 17. Conduction band energy of various models (close up).

C.   IV CURVES

The model was tested and compared with measured results by NRL [16]. The model was run with a 0.3 Al mole fraction under different gate biases. Figure 18 displays the results. The device was subjected to a drain bias ramped from 0.0 to 20.0 Volts with gate biases of 0.0, -1.0, -3.0, and –5.0 Volts.
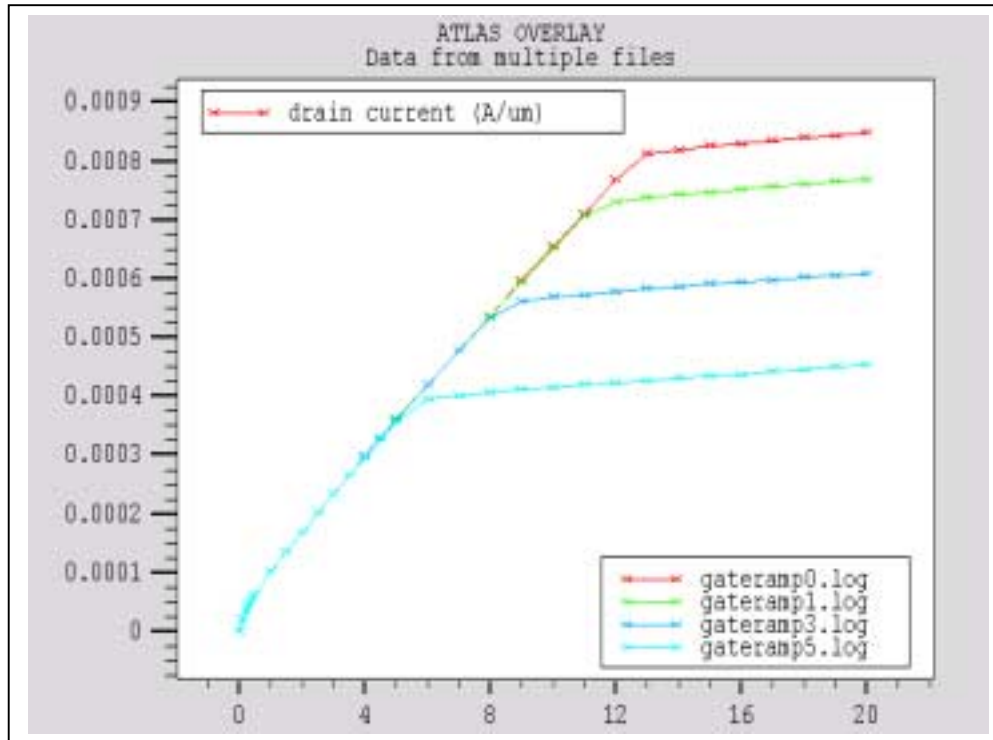
Figure 18. Simulated IV curves for AlGaN HEMT transistor.

NRL's results on a real device are shown in Figure 19.
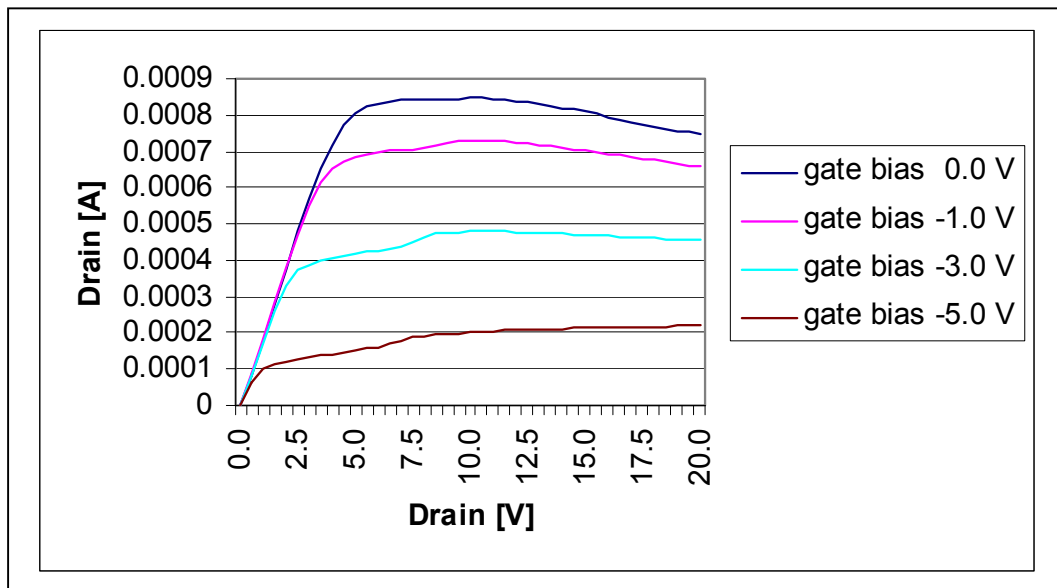
Figure 19. Measured IV curves for AlGaN HEMT transistor.

The model IV curves have noticeable differences. While the real device peaks by five volts on the drain, only the −5.0 gate bias case does so in the model. The real device never surpasses about 0.0009 Amps while the model approaches 0.0012 Amps. The real device curves (except the −5.0 volt case) begin to fall off around thirteen volts on the drain, but the model drain current never fall off. This anomaly is expected to be caused by heating effects for which the model does not account. Despite these differences, the model curves and the real curves are roughly similar and hopefully show promise for using the Silvaco model. Figure 20 shows the simulated and measured results overlaid with the 0.0 V and the −5.0 V gate bias conditions.
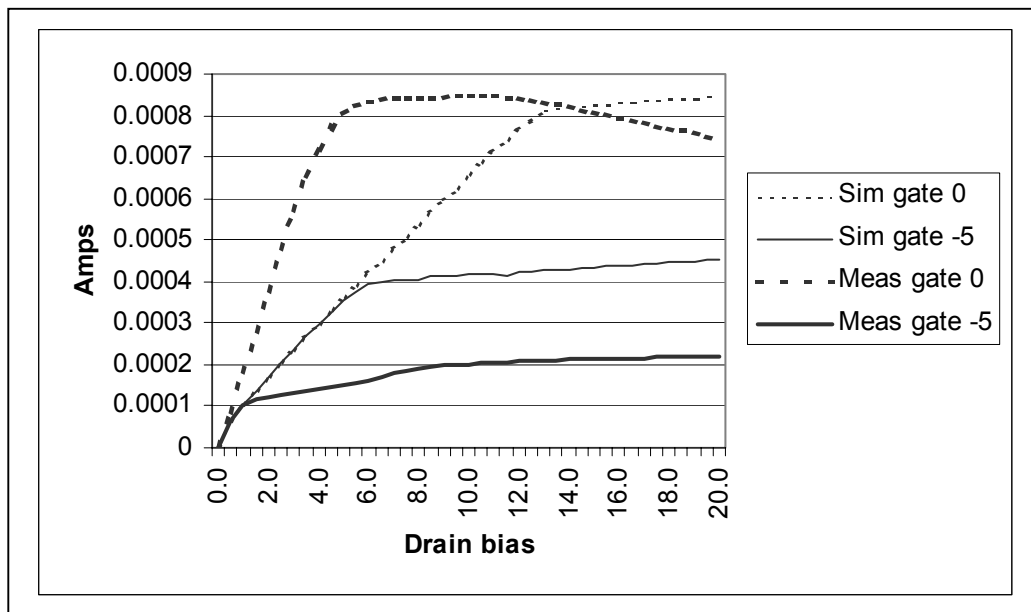
Figure 20. Simulated and measured IV curves for AlGaN HEMT transistor.

IV.   DISCUSSION

The above cutlines demonstrate that appropriate levels of electron sheet concentrations have been achieved at the AlGaN-GaN interface. The model successfully models the impact of various Aluminum mole fractions.

The IV curves demonstrate correspondence between the model and a real device. Some investigation into the differences was conducted. The simulation's slower rise to peak current was thought to be due to leakage current moving through the substrate (not in the 2-DEG channel beneath the AlGaN interface), however, a current flow analysis eliminated that possibility. All current in the device is travelling through the 2-DEG channel. Gate current leakage was also investigated but eliminated as the cause as it is less than 1e-17 (virtual zero). NRL measured gate leakage in actual devices which demonstrated greater leakage (though still negligible) than the simulations. Attempts were made to increase carrier mobility and decrease saturation velocity without satisfactory results. More than a dozen simulations using various mobilities and saturation velocities were run without achieving the steep slope of the measured device from 0.0 to 4.0 volts. A matching peak current of 0.00084 Amps was achieved. An electron mobility of 9000 cm^2/V-sec and electron velocity saturation of 1.1e7 cm/sec were used based on work reported by Eastman in [18].

After exploring options in adjusting electron mobility and velocity saturation, one of two results can be achieved: the steep current rise from 0.0 to 4.0 volts can be matched (but peak current greatly exceeds desired levels), or the peak current can be matched (but the current rise at lower voltages lags behind the desired levels).

Accordingly, other options can be investigated. The thickness of the 2-DEG is currently 0.01 microns. A thinner 2-DEG could be achieved with an adjusted model structure. A structure with less substrate and more focussed meshing (grouping of points within the structure where equilibrium equations are calculated by Silvaco software) would allow a more refined 2-DEG. However, this approach might reduce the effectiveness of a model which includes thermal effects. Without the substrate (sapphire or Silicon Carbide), modeling a device under thermal conditions might suffer in accuracy.

Other means to attack the I-V curve discrepancies are available in Silvaco Software. Some options not used in this work were the ability to model thermal effects, interface effects, and quantum effects. Silvaco software has a program called GIGA^{TM} which extends ATLAS^{TM} to account for lattice heat flow by implementing Wachutka's thermodynamic model. This program would probably assist the accurate modeling of high field effects where the current begins to decrease, though its impact on the low field problems is doubtful. ATLAS^{TM} has an INTERFACE statement that allows one to define the interface charge density. This function might allow a simple method for defining the 2-DEG, but it would preclude the option of automating the density of the 2-DEG which this project has achieved. The INTERFACE statement also modifies the surface recombination velocity and thermionic emission which might not be desired. Quantum effects can be addressed in Silvaco by including solution of Schrodinger's equation (which modifies the normally calculated density of states and carrier concentrations) and/or including equations to correct carrier temperature through quantum potential. The impact of these equations might have an adverse effect on accurate control of the 2-DEG density.

Another issue to consider is the method of modeling the 2-DEG with doping. The method used in this work is expected to be accurate since Silvaco software normally reacts to doping by reducing electron mobility. Since this model takes manual control of mobility, the result should be a device with the correct mobility and extra electrons at the heterojunction. However, a better approach might be to take electrons from other areas in the device. The software would have to move them to the interface and maintain the appropriate level of concentration as predicted by Ambacher. This approach would require some extensive work with Silvaco, as the software does not currently allow such an option.

THIS PAGE INTENTIONALLY LEFT BLANK

VI. CONCLUSIONS AND RECOMMENDATIONS

A. CONCLUSIONS

PZ and spontaneous polarization effects are significant in GaN devices and can be modeled with Silvaco Software. The desired density of current carriers has been related to the mole fraction of Al in AlGaN. The equations of Ambacher et al. are readily implemented by this model. The current versus voltage performance of the modeled device approximates a measured device, however, it requires some treatment before it will closely match actual device performance. Potential areas for correcting the inaccuracies have been discussed.

B. RECOMMENDATIONS

Strenuous attempts to match real device performance could now be performed. Silvaco Software has capabilities to incorporate thermal effects and Silicon Carbide (instead of Sapphire) as a substrate. These are areas of current concern in device fabrication which ONR and industry ought to be attracted to fund such work.

Silvaco Software has expressed interest to incorporate the PZ effect into the BLAZE software module. This effort would aid Navy needs in developing new GaN devices. Future thesis research can be conducted in cooperation with Silvaco to incorporate this work into their software. Specifically, the AlGaN layer thickness and mole fraction composition might be automatically updated from the structure file (to eliminate the need to enter those values into the C-INTERPRETER code). Also the Fermi level might be automatically updated and provided to the C-INTERPRETER function rather than using equation 15.

Applying external stress to devices to optimize the 2-DEG created from the PZ effect offers further enhancement of HEMT performance. UC Berkley has expressed an interest in performing the experiments required to measure this phenomenon. The results of such work could be incorporated into the Silvaco Software.

The modeling of the PZ effect is performed in a static fashion by this work. One could investigate the possibility that a dynamic effect between applied voltage bias and PZ effect occurs. If so, Silvaco may be able to incorporate such an effect to their software.

LIST OF REFERENCES

1. Smith, M.C., Dunleavy, L.P., "Comparison of Solid State, MPM, and TWT Based Transmitters for Spaceborne Applications," Proceedings of IEEE Southeastcon '98, pp. 256-259, April 23, 1998.

2. Gonzalez, Guillermo, *Microwave Transistor Amplifiers: Analysis and Design*, Prentice Hall, New Jersey, 1997, p. 81.

3. Pierret, Robert, *Semiconductor Device Fundamentals*, Addison-Wesley Publishing Company, Massachusetts, 1996, p. 526.

4. Burm, J., "General Remarks on GaN-based Transistors and Potential for High Temperature/Power Operation," Jun 1998, *Properties, Processing and Applications of Gallium Nitride and Related Semiconductors,* INSPEC 1999, p. 569.

5. Jelenski, Andrzej, "Gallium Nitride--New Material for Microwave and Optoelectronics," Microwaves and Radar, MIKON '98, 12th International Conference on , Vol. 4, 1998, pp. 147-158.

6. Takeuchi and Akasaki, "GaInN Quantum Wells: Piezoelectricity," Feb 1998 *Properties, Processing and Applications of Gallium Nitride and Related Semiconductors,* INSPEC 1999, p. 525.

7. Asbeck, P.M., et al, "Piezoelectric Charge Densities in AlGaN/GaN HFETs," *ELECTRONIC LETTERS*, 3 July 1997, Vol. 33, No.14, pp. 1230-1231.

8. Kittel, Charles, *Introduction to Solid State Physics, 5th Edition*, John Wiley & Sons, New York, NY, 1976.

9. Kasap, S.O., *Principles of Electrical Engineering Materials and Devices,* IRWIN, Chicago, IL, 1997.

10. Silvaco International, *ATLAS User's Manual,* November 1998.

11. Haliday, Resnik, Walker, *Fundamentals of Physics 5th Edition,* John Wiley & Sons, New York, NY, 1997.

12. Leszczynski, M, et al, "Lattice Parameters of the Group III Nitrides," Feb 1998 *Properties, Processing and Applications of Gallium Nitride and Related Semiconductors,* INSPEC 1999 p. 6-9.

13. Ambacher, O., et al, "Two Dimensional Electron Gases Induced by Spontaneous and Piezoelectric Polarization in Undoped and Doped AlGaN/GaN Heterostructures," *Journal of Applied Physics,* Vol. 87, Number 1, January 1, 2000, p. 334-344.

14. Shur, Michael, *Physics of Semiconductor Devices,* Prentice Hall, Engelwood Cliffs, NJ, 1990.

15. Dimitrijev, Sima, *Understanding Semiconductor Devices,* Oxford University Press, New York, 2000.

16. Binari, S.C. et al, "Trapping Effects and Microwave Power Performance in AlGaN/GaN HEMTs," unpublished report (expect to be published in *Electron Device Letters*, April 2001)

17. Mohney, S., "Schottky Barrier Contacts to GaN," April 1998, *Properties, Processing and Applications of Gallium Nitride and Related Semiconductors,* INSPEC 1999, p. 496.

18. Eastman, L, "High Power, Broadband, Linear, Solid State Amplifier 1st Annual Report under MURI Contract No. N00014-96-1-1223" Sept. 1, 1996 – Aug. 31, 1997. http://www.iiiv.cornell.edu/www/schaff/muri/reports/fy97annual/ annual_report.html

APPENDIX A. DECKBUILD SIMULATION INPUT DECK

```
#   Program name: resultshemt3.in
#   Program purpose:  Final HEMT design
#                     xcomp (mole fraction of Al in AlGaN) = .3
#   Date:  10 Feb 2001

go atlas

mesh infile=x3.str

doping n.type f.doping=x3.c
 material f.bandcomp=x3.c  \
  f.epsilon=x3.c

material mun=200.0 mup=50

contact name=gate workfun=3.5

models fermidirac

output con.band val.band band.param e.mobility h.mobility

solve init
save outf=x3.plt
tonyplot x3.plt

method block gummel newton maxtrap=10

#solve vgate=0.0 vstep=-0.1 vfinal=-3.0 name=gate vsource=0.0 vdrain=0.0

log outf=resultshemt3.log

solve vdrain=0.0 vstep=0.1 vfinal=0.4 name=drain vsource=0.0 vgate=0.0

solve vdrain=0.0 vstep=0.5 vfinal=5.0 name=drain vsource=0.0 vgate=0.0

solve vdrain=6.0 vstep=1.0 vfinal=20 name=drain vsource=0.0 vgate=0.0

save outf=resultshemt320.plt
tonyplot resultshemt320.plt
tonyplot resultshemt3.log

quit
```

45

THIS PAGE INTENTIONALLY LEFT BLANK

APPENDIX B. C-INTERPRETER FILE

```c
#include <stdio.h>
#include <stdlib.h>
#include <math.h>
#include <ctype.h>
#include <malloc.h>
#include <string.h>

/* FILE NAME:  x3.c*/

/*
 * Composition and temperature dependent electron saturation velocity
 * Statement: MATERIAL
 * Parameter: F.VSATN =
 */
/* electron saturation velocity */
int vsatn(double xcomp,double ycomp,double temp,double *vsn,double *dvsn)
{
return(0);            /* 0 - ok */
}


/*
 * Composition and temperature dependent hole saturation velocity
 * Statement: MATERIAL * Parameter: F.VSATP
 */
 /* hole saturation velocity */
int vsatp(double xcomp,double ycomp,double temp,double *vsn,double *dvsn)
{
        return(0);            /* 0 - ok */
}

/*
 * Electron velocity saturation model.
 * Statement: MATERIAL
 * Parameter: F.MUNSAT
 */
 /* electron velocity saturation */
int munsat(double e,double v,double mu0,double *mu,double *dmde)
 {
        return(0);            /* 0 - ok */
}

 /* electron velocity saturation */
```

```
/*
 * Hole velocity saturation model.
 * Statement: MATERIAL
 * Parameter: F.MUPSAT
 */

int mupsat(double e,double v,double mu0,double *mu,double *dmde)
{
        return(0);           /* 0 - ok */
}

 /* position dependent doping */
/*
 * Position dependent net doping.
 * Statement: DOPING
 * Parameter: F.DOPING */
int doping(double x,double y,double *nnet)
{
        /*Ambacher*/

double xAct, x2, e, epsilon0, dalgan, Efermi, fib, Eg, Eg0, deltaEC;
double epsilonx, r, a0, agan, c13, c33, e31AlN, e31GaN, e33AlN, e33GaN;
double e31, e33, Ppe, Psp, Ppe0, Psp0, sigma, ns;

double nn, nn1, nn2, nn3;


xAct=0.3;   /*mole fraction of Al in AlGaN (must be adjusted manually)*/
x2=xAct;

e=1.60218e-19;       /*[C] charge of an electron*/
epsilon0=8.8542e-12;   /*[C/VM] permittivity of free space*/
dalgan=200e-10;

Efermi=2.1917*x2-0.102967-7*x2*x2*x2*x2*x2*x2;        /* [CV] Fermi level
wrt GaN conduct. band energy*/

fib=1.3*x2+.84;     /*[CV--(eV)] Gate Schottky barrier (work function?)*/
Eg=x2*6.13+(1-x2)*3.42-x2*(1-x2);    /*[CV] AlGaN  bandgap (x2 = Al  mole
fraction)*/
Eg0=3.42;                 /*[CV] GaN bandgap*/
deltaEC=0.7*(Eg-Eg0);        /*[CV] band offset*/
epsilonx=-.3*x2+10.4;         /*[] relative permittivity*/
r;
if (x2<=0.38)
   r=0.0;                /*[] degree of relaxation*/
```

48

```c
if (x2>0.38)
   if (x2<=0.67)
   r=3.5*x2-1.33;


if (x2>0.67)
   r=1.0;



a0=(-0.077*x2+3.189)*1.e-10;  /*[m] AlGaN lattice constant*/
agan=3.189e-10;           /*[m] GaN lattice constant*/
c13=(5*x2+103);            /*[GPa] AlGaN elastic coefficients*/
c33=(-32*x2+405);

e31AlN=-.6;               /*[C/m^2]  PZ coefficients*/
e31GaN=-.49;

e33AlN=1.46;
e33GaN=.73;

e31=(e31AlN-e31GaN)*x2+e31GaN;
e33=(e33AlN-e33GaN)*x2+e33GaN;

/*double e31AlN=-.58;*/              /* alt. PZ coefficients (not used)*/
/*double e31GaN=-.36;*/             /*but mentioned in Ambacher.*/

/*double e33AlN=1.55;*/
/*double e33GaN=1.0;*/

/*double e312=(e31AlN-e31GaN)*x2+e31GaN;*/
/*double e332=(e33AlN-e33GaN)*x2+e33GaN;*/

/*double e31AlN=-.38;*/
/*double e31GaN=-.32;*/

/*double e33AlN=1.29;*/
/*double e33GaN=.63;*/

/*double e313=(e31AlN-e31GaN)*x2+e31GaN;*/
/*double e333=(e33AlN-e33GaN)*x2+e33GaN;*/


Ppe=2*(r-1)*((a0-agan)/a0)*(e31-e33*(c13/c33)); /*PZ polarization*/
Psp=(-0.052*x2-0.029);                 /*Spontaneous polarization*/
```

```
x2=0.0;

e31=(e31AlN-e31GaN)*x2+e31GaN;          /*Resetting constants & coeff.*/
e33=(e33AlN-e33GaN)*x2+e33GaN;          /*for GaN*/
a0=(-0.077*x2+3.189)*1.e-10;
c13=(5*x2+103);
c33=(-32*x2+405);
r=0.0;

Ppe0=2*(r-1)*((a0-agan)/a0)*(e31-e33*(c13/c33));   /*PZ polarization*/
Psp0=(-0.052*x2-0.029);                 /*Spontaneous polarization*/
x2=xAct;

sigma=(Ppe0+Psp0)-(Ppe+Psp);  /*sheet charge per m^2*/
sigma=sigma/1.e4;          /*per cm^2*/

/*electron sheet concentration*/
ns=sigma/e-(epsilon0*epsilonx/(dalgan*e))*(fib+Efermi-deltaEC)/1.e4;


/*e311  Constants measured differently by various researchers*/
/*e312  provided by Ambacher.*/
/*e313      actually used above*/
/*e331*/
/*e332*/
/*e333      actually used above*/


        /*Ambacher*/


        nn1 = 1.e5;
        nn2 = 5.e18;
        nn3 = ns*(1.e6);  //Sheet charge is spread over 0.01 microns, so
        nn = nn1;         //ns [n/cm^2] is multiplied by 1/10^-6 [cm^-1]
                          //in order to translate to [n/cm^3] which
                          //ATLAS requires.

        if (x>1.6 && x<3.7)
         {
        if (y>=-0.02 && y<-0.0025) nn=nn2;
             if (y>=0 && y<=0.01) nn=nn3;
         }
```

```
        *(nnet) = nn;



        return(0);              /* 0 - ok */
}

  /* band parameters */
/*
 * Temperature and composition dependent band parameters
 * Statement: MATERIAL
 * Parameter: F.BANDCOMP
 * Note:  This function can only be used with BLAZE.
 */
int  bandcomp(double  xcomp,double  ycomp,double  temp,double  *eg,double
*chi,double *nc,double *nv,double *degdt)
{
        double egr, chir, ncr, nvr;


        egr = 3.39+xcomp*2.81;
        chir = 2.7-xcomp*2.0;
        ncr = (1.79+xcomp*2.63)*1.e18;
        nvr = (3.31+xcomp*3.45)*1.e18;

    *(eg) = egr;
    *(chi) = chir;
    *(nc) = ncr;
    *(nv) = nvr;

        return(0);              /* 0 - ok */
}

 /* electron mobility */
/*
 * Composition, temperature and doping dependent electron mobility
 * Statement: MATERIAL
 * Parameter: F.CONMUN
*/
int conmun(double xcomp,double ycomp,double temp,double ntot,double *mun)

{
        return(0);              /* 0 - ok */
}

 /* hole mobility */
```

```c
/*
 * Composition, temperature and doping dependent hole mobility
 * Statement: MATERIAL
 * Parameter: F.CONMUP
 */
int conmup(double xcomp,double ycomp,double temp,double ntot,double *mup)
{
        return(0);          /* 0 - ok */
}



 /* relative permittivity */
/*
 * Composition and temperature dependent permittivity.
 * Statement: MATERIAL
 * Parameter: F.EPSILON */
int epsilon(double xcomp,double ycomp,double temp,double *eps)
{
        double epsr;

        epsr = 9.0-xcomp*0.5;

     *(eps) = epsr;

        return(0);          /* 0 - ok */
}



 /* interface fixed charge */
/*
 * Interface fixed charge as a function of position.
 * Statement: INTERFACE
 * Parameter: F.QF
 */
int int_fixed_charge(double x,double y,double *fixed)
{
        return(0);
}



 /* device degradation interface acceptor traps */
/*
 * Interface acceptor trap density as a function of location
 * Statement: DEGREDATIONPARAM
 * Parameter: F.NTA
 */
```

```c
int devdeg_nta(double x,double y,double *nta)
{
        return(0);
}


    /* device degradation interface donor traps */
/*
 * Interface donor trap density as a function of location
 * Statement: DEGREDATIONPARAM
 * Parameter: F.NTD
 */
int devdeg_ntd(double x,double y,double *ntd)
{
        return(0);
}


 /* device degradation electron capture xsect */
/*
 * Interface electron capture cross section
 * Statement: DEGREDATIONPARAM
 * Parameter: F.SIGMAE
 */
int devdeg_sigmae(double x,double y,double *sigmae)
{
        return(0);
}

/* device degradation hole capture xsection */
/*
 * Interface hole capture cross section
 * Statement: DEGREDATIONPARAM
 * Parameter: F.SIGMAH
 */
int devdeg_sigmah(double x,double y,double *sigmah)
{
        return(0);
}

/* interface acceptor traps */
/*
 * Interface acceptor trap density as a function of location
 * Statement: INTTRAP (ACCEPTOR)
 * Parameter: F.DENSITY
 */
int int_acc_trap(double x,double y,double *density)
{
```

```c
        return(0);
}

/* interface donor traps */
/*
 * Interface donor trap density as a function of location
 * Statement: INTTRAP (DONOR)
 * Parameter: F.DENSITY
 */
int int_don_trap(double x,double y,double *density)
{
        return(0);
}

/*
 * Interface donor trap density vs position
 * Statement: INTTRAP
 * Parameter: F.INTDONOR
 */
int    intdonor(double    x,double    y,double    energy,double    *density,double
*ncross,double *pcross,double *nlife,double *plife,double *gd)
{
        return(0);
}

/*
 * Interface acceptor trap density vs position
 * Statement: INTTRAP
 * Parameter: F.INTACCEPTO
 */
int    intacceptor(double    x,double    y,double    energy,double    *density,double
*ncross,double *pcross,double *nlife,double *plife,double *ga)
{
        return(0);
}
```

INITIAL DISTRIBUTION LIST

1. Defense Technical Information Center 2
   8725 John J. Kingman Road, Suite 0944
   Ft. Belvoir, VA 22060-6218

2. Dudley Knox Library 2
   Naval Postgraduate School
   411 Dyer Road
   Monterey, CA 93943-5101

3. Engineering and Technology Curricular Office, Code 34………………………...1
   Naval Postgraduate School
   Monterey, CA 93943-5109

4. Chairman, Code EC………………………………………………………………….1
   Department of Electrical and Computer Engineering
   Naval Postgraduate School
   Monterey, CA 93943-5121

5. Prof. Todd R. Weatherford, Code EC/Wt…………………………………………3
   Department of Electrical and Computer Engineering
   Naval Postgraduate School
   Monterey, CA 93943-5121

6. Dr. Harry Dietrich…………………………………………………………………….2
   Code 6856
   Naval Research Laboratory
   Washington D.C. 20375

7. LT Karl P. Eimers, USN……………………………………………………………..3
   P.O. Box K
   St. Maries, ID 83861